How to calculate linear absorption spectra with lifetime broadening using fewest switches surface hopping trajectories: A simple generalization of ground-state Kubo theory

Andrew S. Petit and Joseph E. Subotnik

Citation: The Journal of Chemical Physics **141**, 014107 (2014); doi: 10.1063/1.4884945
View online: http://dx.doi.org/10.1063/1.4884945
View Table of Contents: http://scitation.aip.org/content/aip/journal/jcp/141/1?ver=pdfcov
Published by the AIP Publishing

How to calculate linear absorption spectra with lifetime broadening using fewest switches surface hopping trajectories: A simple generalization of ground-state Kubo theory

Andrew S. Petit and Joseph E. Subotnik
Department of Chemistry, University of Pennsylvania, 231 S. 34th Street, Philadelphia, Pennsylvania 19104, USA

(Received 21 March 2014; accepted 12 June 2014; published online 3 July 2014)

In this paper, we develop a surface hopping approach for calculating linear absorption spectra using ensembles of classical trajectories propagated on both the ground and excited potential energy surfaces. We demonstrate that our method allows the dipole-dipole correlation function to be determined exactly for the model problem of two shifted, uncoupled harmonic potentials with the same harmonic frequency. For systems where nonadiabatic dynamics and electronic relaxation are present, preliminary results show that our method produces spectra in better agreement with the results of exact quantum dynamics calculations than spectra obtained using the standard ground-state Kubo formalism. As such, our proposed surface hopping approach should find immediate use for modeling condensed phase spectra, especially for expensive calculations using *ab initio* potential energy surfaces. © *2014 AIP Publishing LLC*. [http://dx.doi.org/10.1063/1.4884945]

I. INTRODUCTION

Consider a two-electronic state system described by the Hamiltonian

$$\hat{H} = |g\rangle \hat{H}_g \langle g| + |e\rangle \hat{H}_e \langle e|, \tag{1}$$

where $\hat{H}_g$ and $\hat{H}_e$ are the nuclear Hamiltonians associated with the ground and excited electronic states, respectively. These electronic states are coupled through the transition dipole moment operator,

$$\hat{\mu} = |e\rangle \mu_{eg} \langle g| + |g\rangle \mu_{ge} \langle e|, \tag{2}$$

which we will assume to be independent of nuclear position following the usual Condon approximation. *Note that for the entirety of this paper, we will make the Condon approximation in the diabatic basis.* We will also treat $\hat{\mu}$ as a scalar for brevity. It is well-known that, for such a system, the electronic absorption spectra can be calculated from nuclear wave packet dynamics according to[1,2]

$$\begin{aligned}\alpha(\omega) &\propto \omega(1 - e^{-\beta\hbar\omega}) \\ &\quad \times \mathrm{Re}\left[\int_0^\infty dt e^{i\omega t} \langle \Psi(0)| e^{i\hat{H}t/\hbar} \hat{\mu} e^{-i\hat{H}t/\hbar} \hat{\mu} |\Psi(0)\rangle\right] \\ &= \omega(1 - e^{-\beta\hbar\omega}) |\mu_{eg}|^2 \\ &\quad \times \mathrm{Re}\left[\int_0^\infty dt e^{i\omega t} \langle \chi(0)| e^{i\hat{H}_g t/\hbar} e^{-i\hat{H}_e t/\hbar} |\chi(0)\rangle\right], \end{aligned} \tag{3}$$

where $|\Psi(0)\rangle = |\chi(0)\rangle|g\rangle$, $|\chi(0)\rangle$ is the initial nuclear wave function, and $\beta = k_B^{-1} T^{-1}$. Physically, $e^{-i\hat{H}_g t/\hbar}|\chi(0)\rangle$ and $e^{-i\hat{H}_e t/\hbar}|\chi(0)\rangle$ represent nuclear wave packets propagated on the ground and excited potential energy surfaces (PESs), respectively. Equation (3) relates the linear absorption spectrum to the Fourier transform of the time-dependent overlap of these wave packets. Alternatively, we can view Eq. (3) in terms of the dipole-dipole correlation function, $C_{\mu\mu}(t)$,

$$\begin{aligned}\alpha(\omega) &\propto \omega(1 - e^{-\beta\hbar\omega}) \mathrm{Re}\left[\int_0^\infty dt e^{i\omega t} \langle \Psi(0)| \hat{\mu}(t) \hat{\mu}(0) |\Psi(0)\rangle\right] \\ &= \omega(1 - e^{-\beta\hbar\omega}) \mathrm{Re}\left[\int_0^\infty dt e^{i\omega t} C_{\mu\mu}(t)\right], \end{aligned} \tag{4}$$

where $\hat{\mu}(t) = e^{i\hat{H}t/\hbar} \hat{\mu} e^{-i\hat{H}t/\hbar}$. It is worth noting that Eq. (4) as well as the first line of Eq. (3) are valid with or without the Condon approximation and can be generalized for the case of arbitrarily many (i.e., more than two) excited states coupled to the ground state through the transition dipole moment operator.

A number of semiclassical approaches have been developed to approximate the quantum dynamics present in Eqs. (3) and (4).[2–22,58,59] In the formalism based on the work of Kubo,[9,10] the dipole-dipole correlation function is evaluated according to

$$\begin{aligned} C_{\mu\mu}^{(\mathrm{Kubo})}(t) = |\mu_{eg}|^2 \Bigg\langle \exp\Bigg[-\frac{i}{\hbar} \int_0^t \Big(H_e(\vec{x}^{\,(g)}(t'), \vec{p}^{\,(g)}(t')) \\ - H_g(\vec{x}^{\,(g)}(t'), \vec{p}^{\,(g)}(t')) \Big) dt' \Bigg] \Bigg\rangle_g , \end{aligned} \tag{5}$$

where H_g and H_e are the classical nuclear Hamiltonians for the ground and excited electronic states, respectively, μ_{eg} is the transition dipole moment matrix element coupling these electronic states, and $\langle ... \rangle_g$ denotes averaging over an ensemble of classical trajectories propagated on the ground state surface, $\{(\vec{x}^{\,(g)}(t), \vec{p}^{\,(g)}(t))\}$. Physically, Eq. (5) relates the dipole-dipole correlation function to the ensemble average of a phase factor that follows fluctuations in the energy gap between the ground and excited PESs throughout classical trajectories run on the ground state potential. These fluctuations are due to interactions between the chromophore and

the environment as well as from the vibrational motions of the chromophore itself.

The derivation of Eq. (5) is based on a stochastic and classical treatment of environmental fluctuations.[9] A more rigorous analysis of the semiclassical approximation to Eq. (3) shows that the classical trajectories in Eq. (5) should be propagated on the mean PES, so that[11,15,17,23,24]

$$C_{\mu\mu}^{(\mathrm{mean})}(t) = |\mu_{eg}|^2 \left\langle \exp\left[-\frac{i}{\hbar}\int_0^t \left(H_e(\vec{x}^{\,(\frac{g+e}{2})}(t'), \vec{p}^{\,(\frac{g+e}{2})}(t')) - H_g(\vec{x}^{\,(\frac{g+e}{2})}(t'), \vec{p}^{\,(\frac{g+e}{2})}(t'))\right) dt' \right] \right\rangle_g . \quad (6)$$

In other words, the trajectories in Eq. (6) are evolved using nuclear equations of motion derived from the Hamiltonian $H_{(g+e)/2} = H_g/2 + H_e/2$. Both Eqs. (5) and (6) have been used extensively in the literature to calculate electronic spectra.

One major limitation of both Eqs. (5) and (6) is that these approaches are unable to directly describe the effects of nonadiabatic dynamics and electronic relaxation. Moreover, it is unclear how Eq. (6) should be generalized to account for the presence of multiple, coupled excited electronic states. Theoretical chemistry has a completely different set of semiclassical computational tools for modeling photoinduced electronic relaxation and quantifying branching ratios, including multiple spawning and Tully's fewest switches surface hopping (FSSH).[25–28] In this article, we will focus on FSSH, which has become an especially popular tool for calculating electronic transition rates due to its computational efficiency and algorithmic simplicity.[29–33] Despite the fact that nonadiabatic excited state dynamics can have significant spectroscopic (and photochemical) implications,[34,35] the FSSH algorithm has not yet been fully utilized to calculate electronic spectra. While recent work has focused on incorporating the interaction of molecules with strong laser pulses into the FSSH algorithm,[36–38] to our knowledge, the direct calculation of dipole-dipole correlation functions (and hence spectra) from ensembles of FSSH trajectories has not yet been accomplished.

Given the broad interest in nonadiabatic dynamics and spectroscopy among theoretical chemists, it might be surprising that FSSH dynamics have not yet been used to model electronic spectra directly. Nevertheless, the current state of affairs can be explained by the historical absence of a well-defined FSSH density matrix with which one may calculate electronic observables such as dipole-dipole correlation functions. Many researchers in the past have sought to build up an approximate FSSH density matrix in order to calculate diabatic populations.[39–43] However, because each FSSH trajectory carries both an electronic wave function as well as an active adiabatic surface, some electronic information appears to be effectively double counted. This further complicates the calculation of diabatic populations from FSSH trajectories and although several different approaches have been developed to overcome this complication, none has been fully satisfactory.[39–42] Recently, the problem of properly combining information from the FSSH electronic wave functions and active adiabatic surfaces reappeared two times in a paper by Jansen and co-workers who calculated two-dimensional electronic spectra using FSSH.[44] First, in order to evolve the electronic populations, Jansen *et al.* approximated the nuclear electronic density matrix using both the FSSH wave functions and active adiabatic surfaces as possible starting points (see Ref. 42). Second, Jansen *et al.* propagated the nuclei along the ground state potential during electronic coherences, presumably because of the previous ambiguities underlying FSSH dynamics.[44]

In a series of recent papers, our group demonstrated the correct connection between FSSH and Kapral and Martens' mixed quantum-classical Liouville equation.[23,45–47] In doing so, we obtained a well-defined expression for the mixed quantum-classical nuclear-electronic density matrix that is consistent with a swarm of FSSH trajectories.[48,49] Our analysis makes it clear that information from both FSSH electronic wavefunctions and FSSH active adiabatic surfaces is necessary to build up the proper nuclear-electronic density matrix. Using this FSSH nuclear-electronic density matrix, we believe we can now calculate any electronic property of interest directly from an ensemble of surface hopping trajectories. In this paper, we will use these ideas to calculate dipole-dipole correlation functions from ensembles of FSSH trajectories evolved on the ground and on the excited PESs.

One word of caution is in order. Evaluating dipole-dipole correlation functions represents a major challenge for the FSSH algorithm for two reasons. First, from Eq. (3), the features in a linear absorption spectrum are due to the details of how wave packets evolving on the ground and excited PESs repeatedly separate and come back together. However, it is known that FSSH dynamics cannot fully capture the nuclear quantum effects associated with wave packet separation and recombination, i.e., decoherence and recoherences.[43,48] A more complete discussion of recoherences in the context of FSSH is given in Appendix C. Second, the calculation of the dipole-dipole correlation function must be stable over an extended period of time; short time approximations to the dynamics will not suffice. This is particularly true for gas phase problems where, without an environment with which to interact, $C_{\mu\mu}(t)$ will oscillate forever. In this study, we will focus on calculating the dipole-dipole correlation functions of model gas phase systems as they provide an especially challenging test of the limits of our FSSH-based method.

Here is an outline of the present paper. In Sec. II, we propose a new semiclassical expression for dipole-dipole correlation functions based on averaging together information obtained from ensembles of classical trajectories propagated on the ground and on the excited potential energy surfaces. We will then demonstrate that our approach is exact for the case of two uncoupled, shifted harmonic potentials with identical harmonic frequencies. In Sec. III, we generalize our approach to account for the presence of nonadiabatic dynamics and electronic relaxation using the FSSH nuclear-electronic density matrix. In Sec. IV, we present results. First, we will consider model two-state systems involving shifted harmonic potentials with different harmonic frequencies as well as shifted Morse potentials. Using the results of numerical

simulations, we will show that the spectra calculated using our semiclassical approach are in better agreement with exact quantum dynamics than spectra obtained from Eq. (5). Likewise, our results are comparable to performing the dynamics on the mean potential (Eq. (6)). Second, we will present proof of principle calculations demonstrating that our semiclassical approach is able to capture the effects of excited state, non-adiabatic dynamics on the linear absorption spectra of model three-state systems. Moreover, for such three-state problems, our spectra are shown to be in better agreement with exact quantum dynamics than the spectra obtained using the ground-state Kubo formalism. We conclude in Sec. V.

II. THEORY PART I: SPECTRA IN THE ABSENCE OF ELECTRONIC RELAXATION

A. A new semiclassical expression for dipole-dipole correlation functions

We begin by noting that Eq. (3) is symmetric to dynamics performed on the ground or on the excited PES. This symmetry is not present in the usual ground-state Kubo formalism, Eq. (5). Therefore, in addition to the ground-state Kubo expression for the electronic coherence between the electronic states g and e,

$$\left\langle \sigma_{eg}^{(g)}(t)\right\rangle_g = \left\langle \exp\left[-\frac{i}{\hbar}\int_0^t \left(H_e(\vec{x}^{\,(g)}(t'),\vec{p}^{\,(g)}(t')) - H_g(\vec{x}^{\,(g)}(t'),\vec{p}^{\,(g)}(t'))\right)dt'\right]\right\rangle_g \sigma_{eg}(0), \quad (7)$$

we can also calculate another (excited-state) expression for the electronic coherence

$$\left\langle \sigma_{eg}^{(e)}(t)\right\rangle_g = \left\langle \exp\left[-\frac{i}{\hbar}\int_0^t \left(H_e(\vec{x}^{\,(e)}(t'),\vec{p}^{\,(e)}(t')) - H_g(\vec{x}^{\,(e)}(t'),\vec{p}^{\,(e)}(t'))\right)dt'\right]\right\rangle_g \sigma_{eg}(0). \quad (8)$$

Here, $(\vec{x}^{\,(g)}(t),\vec{p}^{\,(g)}(t))$ and $(\vec{x}^{\,(e)}(t),\vec{p}^{\,(e)}(t))$ represent classical trajectories that are propagated on the ground and on the excited PESs, respectively, while $\sigma_{eg}(0)$ is the initial value of the coherence. In both expressions, $\langle ...\rangle_g$ denotes ensemble averaging over a swarm of trajectories initialized by sampling from the Wigner distribution on the ground PES consistent with the initial conditions.[50,51] Note that by sampling from a Wigner distribution, we ensure that at $t = 0$, the swarm of trajectories provides a Monte Carlo sampling of the phase space distribution consistent with the initial nuclear density matrix. We now postulate that the dipole-dipole correlation function, $C_{\mu\mu}(t)$, can be obtained according to

$$C_{\mu\mu}(t) = |\mu_{eg}|^2 \frac{\sqrt{\left\langle \sigma_{eg}^{(g)}(t)\right\rangle_g \left\langle \sigma_{eg}^{(e)}(t)\right\rangle_g}}{\sigma_{eg}(0)}. \quad (9)$$

Recall that the transition dipole moment between the two electronic states is assumed to be independent of nuclear position. By taking the geometric average of $\langle\sigma_{eg}^{(g)}(t)\rangle_g$ and $\langle\sigma_{eg}^{(e)}(t)\rangle_g$, Eq. (9) includes, in a balanced way, dynamical information obtained on both PESs, a feature that we will later see greatly improves the accuracy of the semiclassical approximation. Empirical justification for Eq. (9) is provided in Subsection II B; see Appendix B for a derivation based on a short time approximation.

B. Equation (9) is exact for two uncoupled, shifted harmonic potentials with identical harmonic frequencies at zero temperature

It is known that Eq. (6) gives the exact lineshape for the model problem of two uncoupled, shifted harmonic potentials with identical harmonic frequencies.[23] We now demonstrate that Eq. (9) also gives the exact lineshape for this model problem. Specifically, we consider the Hamiltonian

$$\begin{aligned} H_g &= \frac{p^2}{2m} + \frac{m\omega_g^2 x^2}{2}, \\ H_e &= \frac{p^2}{2m} + \frac{m\omega_e^2 (x-D)^2}{2} + \epsilon_0, \end{aligned} \quad (10)$$

with $\omega_g = \omega_e = \omega$. Note that in Eq. (10) and the following derivation, we focus on a one-dimensional system for ease of discussion only; the derivation presented below is readily generalized to account for multiple nuclear degrees of freedom.

Evaluating Eqs. (7) and (8) requires the same formal manipulations. Without loss of generality, we will focus on the swarm of trajectories evolving on the excited potential. Each trajectory propagated on the excited PES with initial conditions (x_0, p_0) satisfies

$$x^{(e)}(t) = D + (x_0 - D)\cos(\omega t) + \frac{p_0}{m\omega}\sin(\omega t). \quad (11)$$

Substituting Eq. (11) into Eq. (8), and noting that the kinetic energy terms cancel in the exponential, we find

$$\begin{aligned} \frac{\left\langle \sigma_{eg}^{(e)}(t)\right\rangle_g}{\sigma_{eg}(0)} &= \left\langle \exp\left[-\frac{i}{\hbar}\int_0^t \left(\epsilon_0 - \frac{m\omega^2 D}{2}\left(D - 2D\cos(\omega t') + 2x_0\cos(\omega t')\right) + \frac{2p_0}{m\omega}\sin(\omega t')\right)dt'\right]\right\rangle_g \\ &= \exp\left[-\frac{i\epsilon_0 t}{\hbar} + \frac{im\omega^2 D^2 t}{2\hbar} - \frac{im\omega D^2\sin(\omega t)}{\hbar}\right]\left\langle \exp\left[-\frac{i}{\hbar}\left(Dp_0\cos(\omega t) - Dp_0 - m\omega D x_0\sin(\omega t)\right)\right]\right\rangle_g. \end{aligned} \quad (12)$$

Note that in the second line, we have pulled out a phase factor that is independent of initial conditions and therefore common to all of the trajectories.

In the zero-temperature limit, the initial conditions are sampled from the harmonic oscillator ground state Wigner distribution.[51] The ensemble averaging is therefore accomplished according to

$$\begin{aligned}\left\langle \exp\left[-\frac{i}{\hbar}(Dp_0\cos(\omega t)-Dp_0-m\omega Dx_0\sin(\omega t))\right]\right\rangle_g &= \int_{-\infty}^{\infty}dp_0\int_{-\infty}^{\infty}dx_0\frac{1}{\hbar\pi}\exp\left[-\frac{p_0^2}{m\omega\hbar}-\frac{m\omega x_0^2}{\hbar}\right]\\ &\times\exp\left[-\frac{i}{\hbar}\big(Dp_0(\cos(\omega t)-1)-m\omega Dx_0\sin(\omega t)\big)\right]\\ &= \exp\left[\frac{m\omega D^2}{2\hbar}(\cos(\omega t)-1)\right] \qquad (13)\end{aligned}$$

so that

$$\begin{aligned}\frac{\langle\sigma_{eg}^{(e)}(t)\rangle_g}{\sigma_{eg}(0)} &= \exp\left[-\frac{i\epsilon_0 t}{\hbar}+\frac{im\omega^2D^2t}{2\hbar}-\frac{im\omega D^2\sin(\omega t)}{\hbar}\right]\\ &\times\exp\left[\frac{m\omega D^2}{2\hbar}(\cos(\omega t)-1)\right]. \qquad (14)\end{aligned}$$

Performing the same analysis with the swarm of trajectories evolving on the ground PES leads to

$$\begin{aligned}\frac{\langle\sigma_{eg}^{(g)}(t)\rangle_g}{\sigma_{eg}(0)} &= \exp\left[-\frac{i\epsilon_0 t}{\hbar}-\frac{im\omega^2D^2t}{2\hbar}\right]\\ &\times\exp\left[\frac{m\omega D^2}{2\hbar}(\cos(\omega t)-1)\right]. \qquad (15)\end{aligned}$$

Note that $\langle\sigma_{eg}^{(g)}(t)\rangle_g$ and $\langle\sigma_{eg}^{(e)}(t)\rangle_g$ have the same norms but differ substantially in their phases. Substituting Eqs. (14) and (15) into Eq. (9), we obtain the well-known exact, fully quantum mechanical result for this model system,[13,14]

$$\begin{aligned}C_{\mu\mu}(t) &= |\mu_{eg}|^2\exp\left[-\frac{i\epsilon_0 t}{\hbar}\right]\\ &\times\exp\left[-\frac{im\omega D^2}{2\hbar}\sin(\omega t)+\frac{m\omega D^2}{2\hbar}(\cos(\omega t)-1)\right]. \qquad (16)\end{aligned}$$

The importance of including dynamical information obtained from trajectories propagated on both PESs is evident by considering the effect of using only Eq. (7) or (8) to approximate $C_{\mu\mu}(t)$. For example, the dipole-dipole correlation function obtained using the ground-state Kubo approach is directly proportional to Eq. (15) and therefore exhibits a phase that differs significantly from the exact result. Finally, note that a generalization of this derivation to finite-temperatures can be found in Appendix A.

III. THEORY PART II: SPECTRA WITH ELECTRONIC RELAXATION

We now extend the approach developed above to account for the presence of non-adiabatic dynamics. In doing so, we will propagate swarms of trajectories using Tully's fewest switches surface hopping (FSSH) procedure.[25] In order to develop an expression for the dipole-dipole correlation function, we will make use of the recently developed definition of the nuclear-electronic density matrix consistent with an ensemble of FSSH trajectories.[48,49] As FSSH has been extensively discussed in the literature, we will not provide a description of it here.[25,48,52]

In the formalism developed in this section, we will consider systems for which, in the *diabatic representation*, the transition dipole moment is position independent and couples the ground state to a single (bright) excited state. However, the bright excited state is vibronically coupled to one or more dark excited states as well as, in general, also to the ground state. From the above discussion, we will clearly need to evolve two ensembles of FSSH trajectories: one ensemble initialized on the ground diabatic state (state 1) and the other ensemble initialized on the bright diabatic excited state (state 2). The initial electronic wave function for all of the trajectories (in the *diabatic representation*) is taken to be a coherent superposition of the ground and bright states with coefficients at $t = 0$ given by $b_1(0) = b_2(0) = 1/\sqrt{2}$ and $b_{k>2}(0) = 0$.

Because FSSH dynamics shall be performed in the *adiabatic representation*, we must now describe how to initialize the FSSH trajectories in practice as well as how to construct the adiabatic transition dipole moment operator. The adiabatic, $\{|\Phi_i\rangle\}$, and diabatic, $\{|\Xi_a\rangle\}$, bases are related by a position-dependent unitary transformation, $\mathbf{U}(\vec{x})$, and the electronic wave function for the ℓth trajectory, $|\psi^{[\ell]}\rangle$, can be expressed in either basis as

$$\begin{aligned}|\psi^{[\ell]}\rangle &= \sum_i c_i^{[\ell]}|\Phi_i\rangle\\ &= \sum_i\sum_a U_{ai}(\vec{x}^{\,[\ell]})c_i^{[\ell]}|\Xi_a\rangle = \sum_a b_a^{[\ell]}|\Xi_a\rangle. \qquad (17)\end{aligned}$$

With this in mind, the active adiabatic potential for the ℓth trajectory, $\lambda^{[\ell]}(0)$, is stochastically determined based on the relative values of the adiabatic expansion coefficients $|c_i^{[\ell]}(0)|^2$. In a similar manner, the transition dipole moment operator is transformed into the adiabatic representation according to

$$\hat{\mu}^{(\mathrm{adiab})}(\vec{x}) = \mathbf{U}^{\dagger}(\vec{x})\hat{\mu}^{(\mathrm{diab})}\mathbf{U}(\vec{x}). \qquad (18)$$

Note that because of the position-dependence of $\mathbf{U}(\vec{x})$, the transition dipole moment operator is non-Condon in the adiabatic representation.

We now consider how to evaluate Eqs. (7) and (8) as a Monte Carlo average over swarms of independent FSSH trajectories using the FSSH nuclear-electronic density matrix, $\mathbf{A}(\vec{x}, \vec{p}, t)$, expressed at each geometry in terms of the adiabatic electronic basis for that geometry. In doing so, we first note that the off-diagonal elements of the electronic density matrix carried by the FSSH trajectories, $\sigma_{jk}^{[\ell]}(t) = c_j^{[\ell]}(t)c_k^{[\ell]*}(t)$, oscillate based on the same time-dependent energy gaps as in Eqs. (7) and (8). Turning to the Monte Carlo integration, we encounter a subtle question of how to properly combine the electronic wave function information with the identity of the active adiabatic surface of each

of the FSSH trajectories. Indeed, while the diagonal elements of $\mathbf{A}(\vec{x}, \vec{p}, t)$ are well-defined in terms of an ensemble of N_{traj} FSSH trajectories with active surfaces $\{\lambda^{[\ell]}(t)\}$ as

$$A_{jj}(\vec{x}, \vec{p}, t) = \frac{1}{N_{\text{traj}}} \sum_{\ell=1}^{N_{\text{traj}}} \delta(\vec{x} - \vec{x}^{\,[\ell]}(t))\delta(\vec{p} - \vec{p}^{\,[\ell]}(t))\delta_{j\lambda^{[\ell]}(t)}, \tag{19}$$

Refs. 46 and 47 give two possible definitions for the off-diagonal elements,

$$\begin{aligned} A^{(j)}_{jk}(\vec{x}, \vec{p}, t) &= \frac{1}{N_{\text{traj}}} \sum_{\ell=1}^{N_{\text{traj}}} \delta(\vec{x} - \vec{x}^{\,[\ell]}(t))\delta(\vec{p} - \vec{p}^{\,[\ell]}(t)) \frac{\sigma^{[\ell]}_{jk}(t)}{\sigma^{[\ell]}_{jj}(t)} \delta_{j\lambda^{[\ell]}(t)}, \\ A^{(k)}_{jk}(\vec{x}, \vec{p}, t) &= \frac{1}{N_{\text{traj}}} \sum_{\ell=1}^{N_{\text{traj}}} \delta(\vec{x} - \vec{x}^{\,[\ell]}(t))\delta(\vec{p} - \vec{p}^{\,[\ell]}(t)) \frac{\sigma^{[\ell]}_{jk}(t)}{\sigma^{[\ell]}_{kk}(t)} \delta_{k\lambda^{[\ell]}(t)}. \end{aligned} \tag{20}$$

Here, $A^{(j)}_{jk}(\vec{x}, \vec{p}, t)$ is defined such that only trajectories that are moving on the jth adiabatic surface at time t contribute to the Monte Carlo sum. Likewise, only the trajectories that are moving on the kth adiabatic surface at time t contribute to $A^{(k)}_{jk}(\vec{x}, \vec{p}, t)$. Although these two definitions should be equivalent, they will not formally agree when represented using independent FSSH trajectories (which is one reason why decoherence should be added to the FSSH algorithm). An ensemble of interacting trajectories would be required to ensure that $A^{(j)}_{jk}(\vec{x}, \vec{p}, t) = A^{(k)}_{jk}(\vec{x}, \vec{p}, t)$ for all times.[48] As a tractable approximation, we will use the following definition for the elements of $\mathbf{A}(\vec{x}, \vec{p}, t)$ in this work:

$$\begin{aligned} A_{jk}(\vec{x}, \vec{p}, t) = \frac{1}{N_{\text{traj}}} \sum_{\ell=1}^{N_{\text{traj}}} &\delta(\vec{x} - \vec{x}^{\,[\ell]}(t))\delta(\vec{p} - \vec{p}^{\,[\ell]}(t)) \\ &\times \frac{\sigma^{[\ell]}_{jk}(t)}{\sigma^{[\ell]}_{jj}(t) + \sigma^{[\ell]}_{kk}(t)} (\delta_{j\lambda^{[\ell]}(t)} + \delta_{k\lambda^{[\ell]}(t)}). \end{aligned} \tag{21}$$

Note that Eq. (21) reduces to the same expression as Eq. (19) for the diagonal matrix elements. For the off-diagonal elements, it generalizes the two definitions in Eq. (20) such that the jth and kth adiabatic electronic states are treated in a balanced way while ensuring that only trajectories moving along either the jth or kth PES at time t contribute to the calculated coherence.[48,49]

Armed with the full nuclear-electronic density matrix, $\mathbf{A}$, our next step is to convert the problem into a *diabatic basis*. After all, the electronic coherence that will enter into Eq. (9) is between the ground and bright excited *diabatic states*. Using Eq. (17), the FSSH nuclear-electronic density matrix in the diabatic representation, $\mathbf{B}(\vec{x}, \vec{p}, t)$, is obtained according to

$$\mathbf{B}(\vec{x}, \vec{p}, t) = \mathbf{U}(\vec{x})\mathbf{A}(\vec{x}, \vec{p}, t)\mathbf{U}^{\dagger}(\vec{x}). \tag{22}$$

The electronic coherence between the ground and bright excited diabatic states associated with a swarm of FSSH trajectories, $\langle \sigma^{(\text{diab})}_{21}(t) \rangle$, is then calculated using

$$\begin{aligned} &\left\langle \sigma^{(\text{diab})}_{21}(t) \right\rangle \\ &= \int_{-\infty}^{\infty} d^{3N}x \int_{-\infty}^{\infty} d^{3N}p \left(\sum_{jk} U_{2j}(\vec{x}) U^{*}_{1k}(\vec{x}) A_{jk}(\vec{x}, \vec{p}, t) \right) \\ &= \frac{1}{N_{\text{traj}}} \sum_{\ell=1}^{N_{\text{traj}}} \sum_{jk} U_{2j}\left(\vec{x}^{\,[\ell]}(t)\right) U^{*}_{1k}\left(\vec{x}^{\,[\ell]}(t)\right) \\ &\quad \times \frac{\sigma^{[\ell]}_{jk}(t)}{\sigma^{[\ell]}_{jj}(t) + \sigma^{[\ell]}_{kk}(t)} (\delta_{j\lambda^{[\ell]}(t)} + \delta_{k\lambda^{[\ell]}(t)}), \end{aligned} \tag{23}$$

where $\sigma^{(\text{diab})}_{21}(0) = 1/2$ based on the initial conditions described above. In practice, we evaluate Eq. (23) using separate swarms of FSSH trajectories initialized on the ground and on the bright excited diabatic PESs to obtain $\langle \sigma^{(\text{diab, g})}_{21}(t) \rangle$ and $\langle \sigma^{(\text{diab, e})}_{21}(t) \rangle$. As in Eq. (9), the dipole-dipole correlation function is then given by

$$C_{\mu\mu}(t) = |\mu^{(\text{diab})}_{21}|^2 \frac{\sqrt{\left\langle \sigma^{(\text{diab, g})}_{21}(t) \right\rangle \left\langle \sigma^{(\text{diab, e})}_{21}(t) \right\rangle}}{\sigma^{(\text{diab})}_{21}(0)}. \tag{24}$$

In Appendix B, we show that the dynamics of Eq. (24) agrees with the results of a rigorous semiclassical analysis of Eq. (3) for short times.

IV. RESULTS AND DISCUSSION

A. Two shifted harmonic potentials with different harmonic frequencies

We first consider the model problem of two shifted harmonic potentials as described in Eq. (10) with $\omega_g \neq \omega_e$, $\omega_g = 3000\ \text{cm}^{-1}$, $m = 1728.26$ a.u., and $\epsilon_0 = 5.0$ hartree. For all of the calculations, the dynamics were run for $t_{\max} = 1000$ a.u. with a time step of $\delta t = 0.02$ a.u. The linear absorption spectra were obtained from $C_{\mu\mu}(t)$ using

$$\alpha(\omega) \simeq -\frac{8\pi\omega}{c\hbar} \text{Im} \left[\int_0^{t_{\max}} e^{i\omega t} \text{Im}\left[C_{\mu\mu}(t)\right] \cos\left(\frac{\pi t}{2t_{\max}}\right) dt \right], \tag{25}$$

where the factor $\cos(\pi t/2t_{\max})$ was used to reduce the presence of spurious Gibbs oscillations by forcing the integrand to smoothly go to zero at the final time included in the dynamics, $t_{\max}$.[53] The spectra were calculated on a frequency grid with a resolution of $\delta\omega = 1200^{-1}$ hartree. The full quantum dynamics results were obtained by evaluating

$$\begin{aligned} &C_{\mu\mu}(t) \\ &= |\mu_{eg}|^2 \sum_j e^{-\beta(E^{(g)}_j - E^{(g)}_0)} \sum_k \left| \left\langle \chi^{(g)}_j \middle| \chi^{(e)}_k \right\rangle \right|^2 e^{-it(E^{(e)}_k - E^{(g)}_j)/\hbar}, \end{aligned} \tag{26}$$

where $|\chi^{(g)}_j\rangle$ is the jth vibrational eigenstate on the ground PES with energy $E^{(g)}_j$ and $|\chi^{(e)}_k\rangle$ is the kth vibrational eigenstate on the excited PES with energy $E^{(e)}_k$. For the

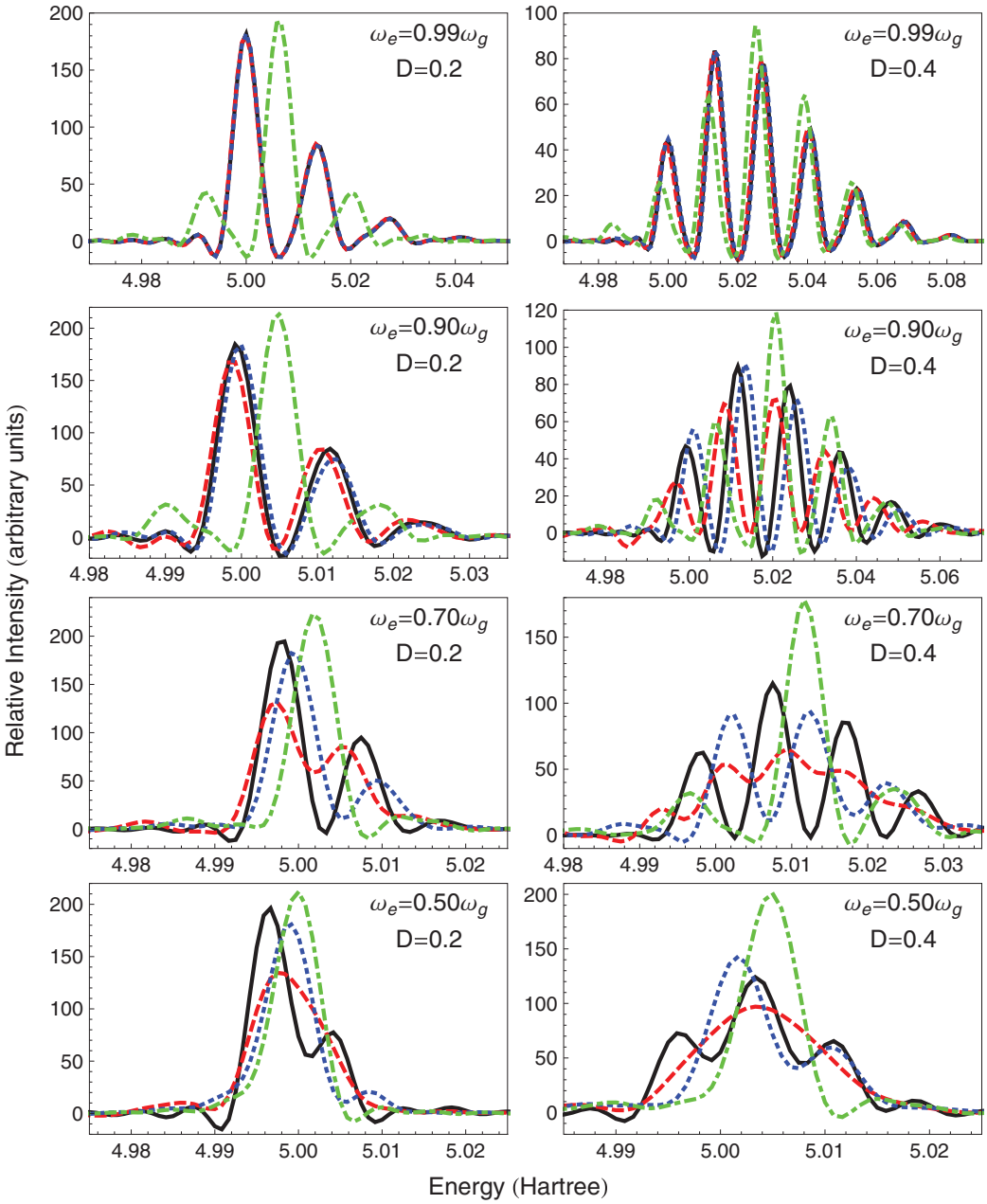

FIG. 1. Comparison between the ($T = 0$) linear absorption spectra of two shifted harmonic potentials with different harmonic frequencies, Eq. (10), as calculated using full quantum dynamics (solid black line), semiclassically using our approach, Eq. (9) (dashed red line), semiclassically with trajectories run on the mean potential, Eq. (6) (dotted blue line), and semiclassically using the ground-state Kubo approach, Eq. (5) (dashed-dotted-dashed green line). Note that in the top two panels, the black curves lie directly below the dashed red and dotted blue lines. A more exhaustive comparison of the semiclassical methods for this model system can be found in the supplementary material.[55]

semiclassical calculations, we used an ensemble of 80 000 trajectories and integrated the equations of motion using the fourth-order Runge Kutta algorithm.[54] Finally, note that in our approach, the sign of $C_{\mu\mu}(t + \delta t)$ was chosen by determining which of the two roots of Eq. (9) lie closest in the complex plane to $C_{\mu\mu}(t)$.

In Figure 1, we present the ($T = 0$) linear absorption spectra of the shifted harmonic potentials model with $\omega_g \neq \omega_e$, as calculated using full quantum dynamics and using the semiclassical method developed in this study (Eq. (9)). We also consider in Figure 1 the alternative semiclassical approaches given in Eqs. (5) and (6). Note that the use of a finite $t_{\max}$ in Eq. (25) introduces artificial linewidths and spurious Gibbs oscillations consistently among the semiclassical and the exact spectra. For all four values of ω_e, the spectra calculated using the ground-state Kubo approach demonstrate the largest deviations from the exact spectra.[9,10] As shown in the supplementary material, this is particularly true for intermediate values of D, that is, $D \simeq 0.2$ a.u.[55] When $\omega_e = 0.99\omega_g$, the semiclassical spectra obtained using our approach as well as using Eq. (6) are in essentially quantitative agreement with the full quantum dynamics results. As ω_e is further reduced, the agreement between the semiclassical and exact spectra decreases. These deviations likely result from the neglect of nuclear quantum effects in both Eqs. (6) and (9). However, the accuracy of our approach

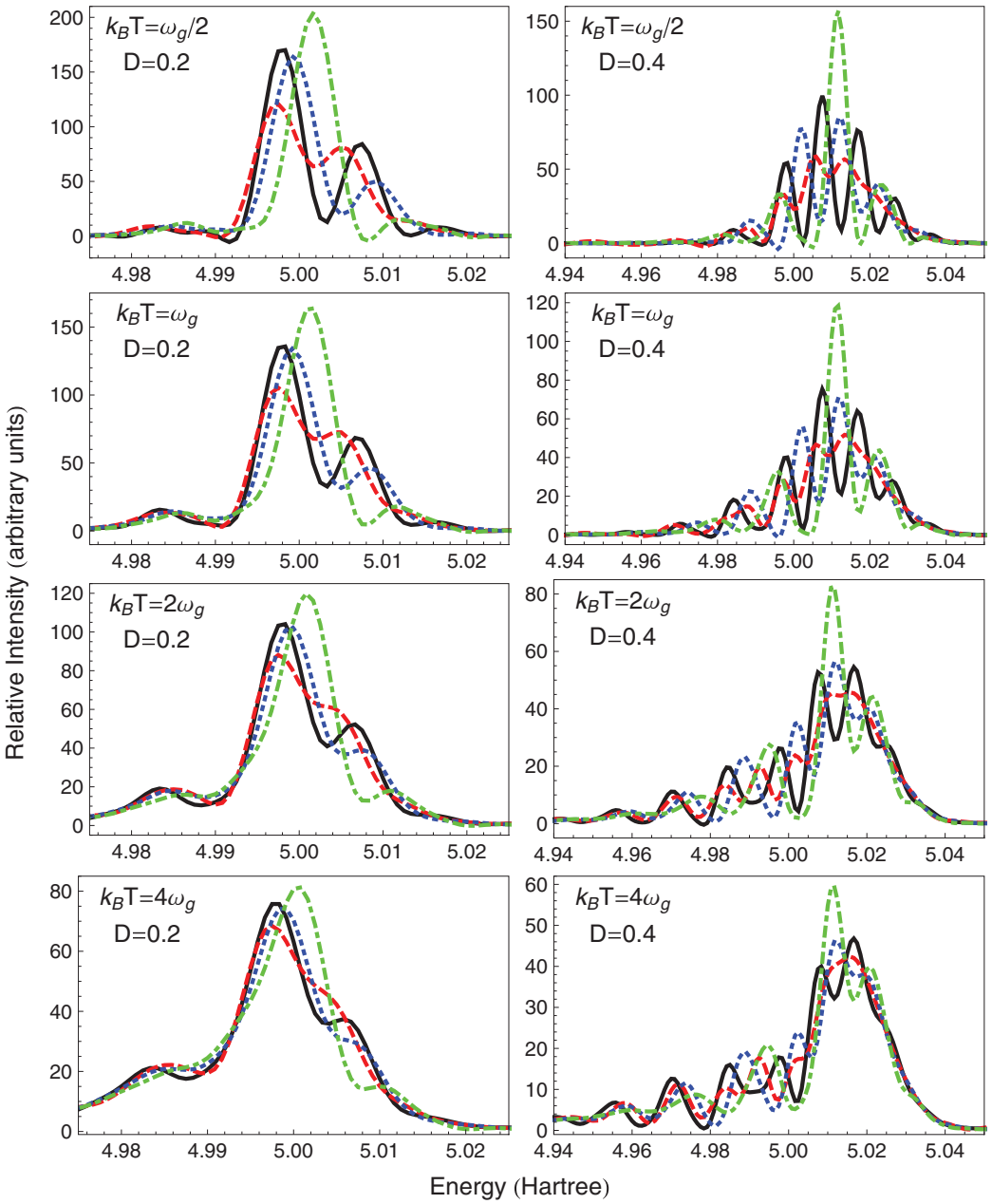

FIG. 2. Comparison between the temperature dependence of the linear absorption spectra of two shifted harmonic potentials, Eq. (10), with $\omega_g = 3000\ \text{cm}^{-1}$ and $\omega_e = 0.7\omega_g$ as calculated using full quantum dynamics (solid black line), semiclassically using our approach, Eq. (9) (dashed red line), semiclassically with trajectories run on the mean potential, Eq. (6) (dotted blue line), and semiclassically using the ground-state Kubo approach, Eq. (5) (dashed-dotted-dashed green line). A more exhaustive comparison of the semiclassical methods for this model system at finite temperatures can be found in the supplementary material.[55]

remains comparable to that of performing the dynamics on the mean potential. It is worth noting that when $\omega_e = 0.5\omega_g$, Eq. (9) better captures the overall spectral lineshape and width than Eq. (6) but misses some of the vibrational structure that performing the dynamics on the mean potential seems to pick up.

The temperature dependence of the linear absorption spectra of the shifted harmonic potentials model with $\omega_e = 0.70\omega_g$, $D = 0.2$, or $D = 0.4$ a.u. (and temperatures ranging from $k_BT = \omega_g/2$ to $k_BT = 4\omega_g$) is illustrated in Figure 2. The initial positions and momenta for all of the semiclassical calculations were sampled from the finite temperature harmonic oscillator Wigner distribution.[1] As shown in the supplementary material, sampling instead from the classical thermal phase space distribution generates the same spectral lineshapes for $k_BT \gtrsim \omega_g$.[55] Focusing now on the data in the figure, the overall agreement between the semiclassical and exact spectra is seen to generally improve with increasing temperature. This is to be expected as nuclear quantum effects are most pronounced when the thermal energy is much less than the spacing between the quantized vibrational energy levels. As in Figure 1, the ground-state Kubo spectra consistently display the largest deviations from the exact spectral lineshapes. The approach developed in this study continues to exhibit comparable accuracy to performing the dynamics on the mean surface.

Before finishing, we note that the magnitude of the oscillations in the norm of $C_{\mu\mu}(t)$ increases as the ground and excited PESs are shifted further apart (not shown). Indeed, with sufficiently large values of D, which for this model is found to be $D \gtrsim 0.4$ a.u., $|C_{\mu\mu}(t)|$ reaches values very close to zero. When $|C_{\mu\mu}(t)| \simeq 0.0$, the phase of the dipole-dipole correlation function obtained using Eq. (9) can become unstable, particularly if the magnitude of the dipole-dipole correlation function remains close to zero for an extended period of time between oscillation periods. This numerical instability can result in a slower convergence of the semiclassical spectra with respect to the number of trajectories included in the ensemble as well as errors in the vibrational structure of the lineshape. Note that such numerical instabilities did not appear for any of the parameter sets considered in this article. Finally, we emphasize that this difficult behavior will be much less pronounced in more realistic, condensed phase systems where interactions with the environment will damp out the long time oscillations in $|C_{\mu\mu}(t)|$.

B. Two shifted Morse potentials

We now consider how the inclusion of anharmonicity affects the semiclassical approach developed in this study (Eq. (9)) by calculating the $T = 0$ linear absorption spectra of a pair of shifted Morse potentials,[56]

$$H_g = \frac{p^2}{2m} + d_e(1 - \exp(-\gamma x))^2,$$
$$H_e = \frac{p^2}{2m} + d_e(1 - \exp(-\gamma(x - D)))^2 + \epsilon_0, \tag{27}$$

where $d_e = (\hbar\omega)/(4\alpha_{anh})$, $\gamma = \sqrt{2m\omega\alpha_{anh}/\hbar}$, and the anharmonicity parameter α_{anh} is defined such that the vth vibrational eigenstate has energy

$$E_v = \hbar\omega\left(v + \frac{1}{2}\right) - \alpha_{anh}\hbar\omega\left(v + \frac{1}{2}\right)^2. \tag{28}$$

The specific parameters of Eq. (27) used in this study are $\omega = 3000\ \text{cm}^{-1}$, $m = 1728.26$ a.u., and $\epsilon_0 = 5.0$ hartree. The eigenstates required to evaluate Eq. (26) were determined using the discrete variable representation (DVR) in the sinc-DVR basis with a grid of 1600 evenly spaced points ranging from -8.0 a.u. to 8.0 a.u.[57] All other simulation details were identical to those used with the previous model.

Figure 3 presents the linear absorption spectra for this model with choices of the anharmonicity constant, $\alpha_{anh} = 0.0001$ and $\alpha_{anh} = 0.01$, that correspond to the potentials supporting 4999 and 49 bound vibrational states, respectively. As with the model of two shifted harmonic potentials, the ground-state Kubo spectra exhibit pronounced deviations from the spectra obtained from full quantum dynamics. This is particularly true when $D = 0.2$ a.u. where Eq. (5) yields a qualitatively incorrect lineshape. When $\alpha_{anh} = 0.0001$, the spectra calculated using our approach are comparable to the spectra obtained by performing the dynamics on the mean PES and in excellent agreement with the spectra calculated using full quantum dynamics. This is unsurprising given that these potentials are quite harmonic in the region of position space sampled by the trajectories. Increasing the anharmonicity by two orders of magnitude does reduce the agreement between the semiclassical and exact spectra but both our semiclassical calculations (Eq. (9)) and those performed on the mean PES (Eq. (6)) do capture the overall lineshapes as well as much of the vibrational structure. Moreover, our approach performs comparably with Eq. (6) when $D = 0.2$ a.u. and is in better agreement with the exact results than Eq. (6) when $D = 0.4$ a.u.

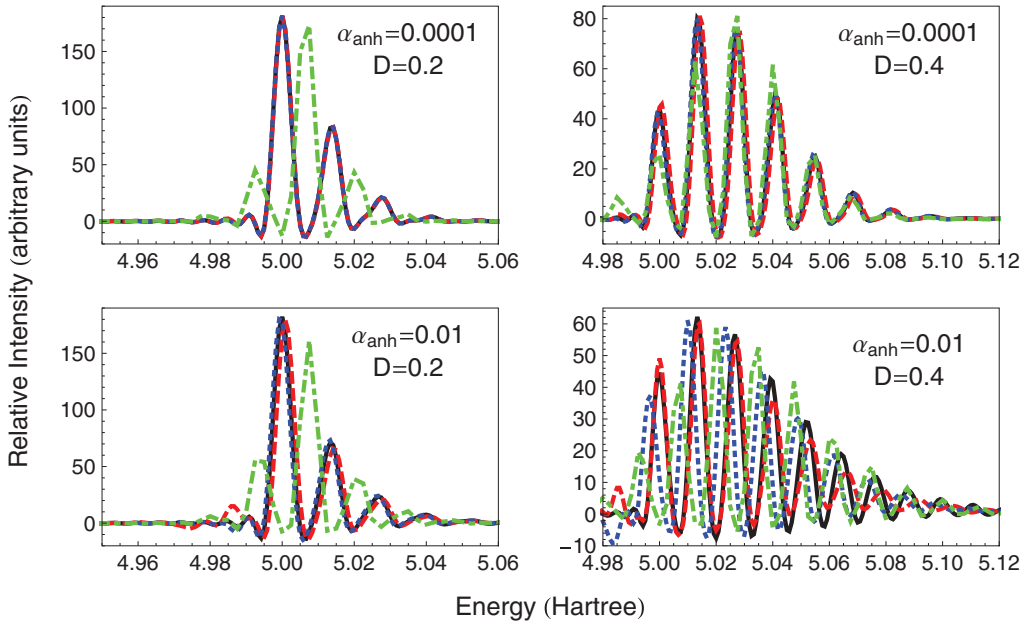

FIG. 3. Comparison between the ($T = 0$) linear absorption spectra of two shifted Morse potentials, Eq. (27), as calculated using exact quantum dynamics (solid black line), semiclassically using our approach, Eq. (9) (dashed red line), semiclassically with trajectories run on the mean potential, Eq. (6) (dotted blue line), and semiclassically using the ground-state Kubo approach, Eq. (5) (dashed-dotted-dashed green line).

C. Non-adiabatic three-state model

We finally consider a three-state model in which, in the *diabatic representation*, the ground and bright states are shifted harmonic potentials while the dark excited state is a repulsive potential that crosses the bright state in the Franck-Condon region. Specifically, the diabatic potentials are taken to be

$$\begin{aligned} V_1(x) &= \frac{m\omega^2 x^2}{2}, \\ V_2(x) &= \frac{m\omega^2 (x - D_2)^2}{2} + \epsilon_2, \\ V_3(x) &= \left(\frac{m\omega^2 (x - D_2 - D_3)^2}{2} + \epsilon_2\right) \\ &\quad \times (1 - \mathrm{erf}(2(x - D_3))) + \mathrm{erf}(2(x - D_3))\epsilon_3, \end{aligned} \tag{29}$$

with $\omega = 3000\ \mathrm{cm}^{-1}$, $m = 1728.26$ a.u., $D_2 = 0.1$ a.u., $D_3 = 0.2$ a.u., $\epsilon_2 = 0.1$ hartree, and $\epsilon_3 = 0.09$ hartree. The bright and dark states are coupled by a constant diabatic coupling, V_{23}, while no such coupling is assumed to exist between the ground state and either excited state ($V_{12} = V_{13} = 0$). Figure 4 shows the adiabatic potentials for three values of V_{23} considered in this study, which range from the diabatic to the adiabatic limits. Also shown in the figure are the adiabatic transition dipole moments calculated using Eq. (18). The adiabatic transition dipole moments, $\mu_{jk}^{(\mathrm{adiab})}(x)$, were made continuous by defining the signs of the columns of $\mathbf{U}(x)$ such that $U_{22}(x) > 0$ and $U_{33}(x) > 0$.

For all of the approaches used to calculate the spectra of the three-state models, the dynamics were propagated for $t_{\max} = 32\,000$ a.u. with a time step of $\delta t = 0.5$ a.u., and using a fourth-order Runge Kutta integration scheme.[54] The spectra were calculated on a frequency grid using Eq. (25) with a spacing of $\delta\omega = 2 \times 10^{-5}$ hartree. An ensemble of 80 000 trajectories were used in the semiclassical calculations. The vibronic eigenstates required to calculate the dipole-dipole correlation function using Eq. (26) were obtained using a DVR grid with 5500 points ranging from −6.0 to 104.0 a.u.[57] Note that the use of a very large grid was required because $V_3(x)$ is a repulsive potential and therefore its vibrational eigenstates are all unbound. Finally, only $T = 0$ spectra for these systems are considered in this study.

In the semiclassical calculations of the three-state models, we found it necessary to adjust the size of the time step in order to ensure accurate integration of the equations of motion, particularly in the diabatic curve crossing region. Specifically, if the energy of a trajectory drifted significantly within a single time step, then the integration of the nuclear equations of motion over that time step was repeated using a series of smaller time steps to ensure energy conservation. Additionally, before evolving the electronic wave functions in

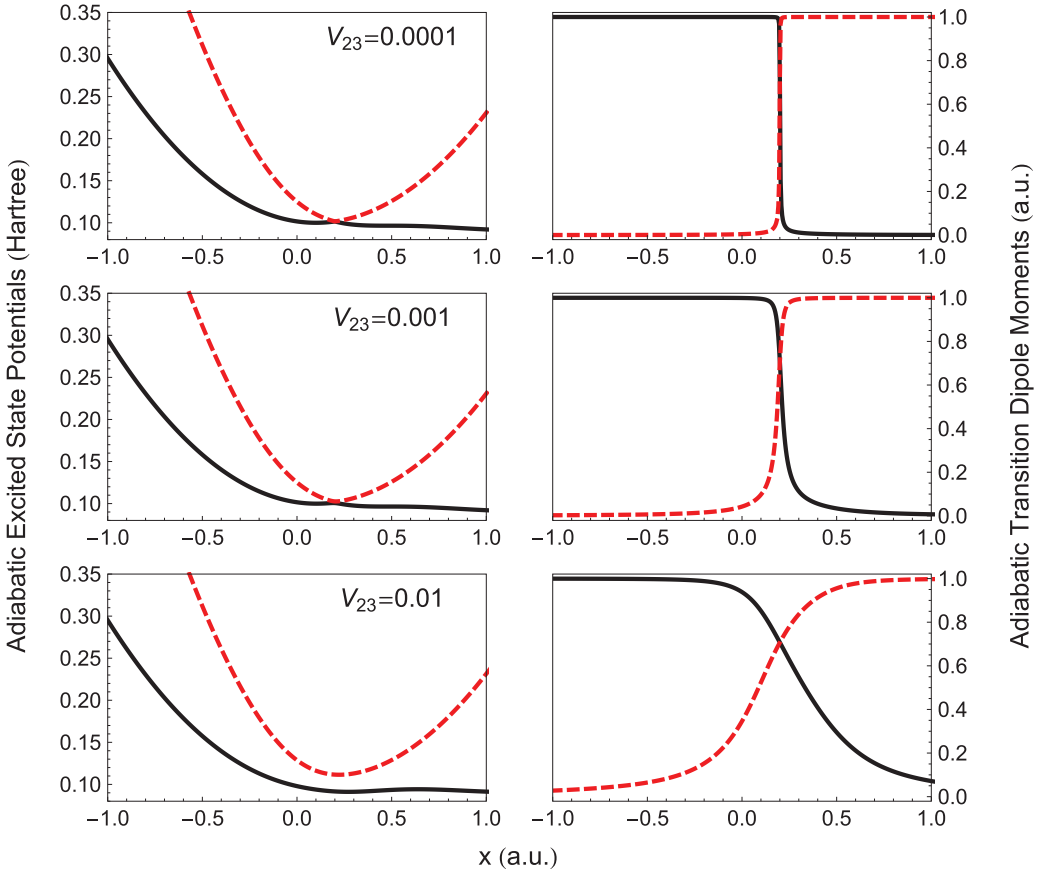

FIG. 4. Adiabatic potentials for the dissociative excited (solid black lines) and bound excited (dashed red lines) electronic states are shown for the three-state models, Eq. (29), with diabatic coupling strengths $V_{23} = 0.0001$, $V_{23} = 0.001$, and $V_{23} = 0.01$ hartree. The non-interacting ground state potential is shown in solid gray lines. Also shown in the right column are the adiabatic transition dipole moments coupling the ground state to the dissociative excited state (black lines) and to the bound excited state (dashed red lines).

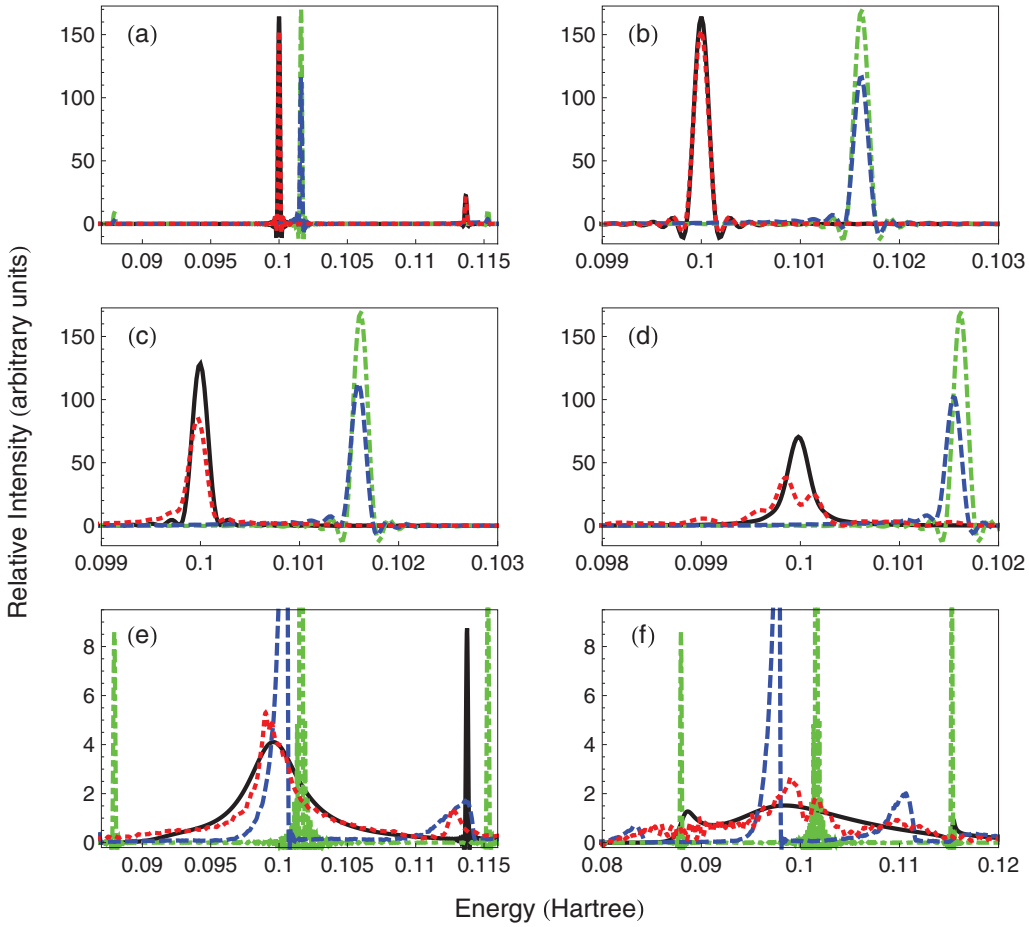

FIG. 5. A comparison between the ($T = 0$) linear absorption spectra of the three-state models calculated using full quantum dynamics (solid black line), semiclassically using Eqs. (23) and (24) (dotted red line), semiclassically using the ground-state Kubo approach in the adiabatic representation (dashed blue line), and semiclassically using the ground-state Kubo approach in the diabatic representation (dashed-dotted-dashed green line). The spectra shown in panels (a) and (b) are for $V_{23} = 0.0001$ hartree with different scales on the abscissa axes while the other panels show relevant spectral regions for (c) $V_{23} = 0.0005$, (d) $V_{23} = 0.001$, (e) $V_{23} = 0.005$, and (f) $V_{23} = 0.01$ hartree.

the FSSH calculations, we identified $h\nu_{\max}$ as the magnitude of the largest element of the electronic Hamiltonian matrix in the time-dependent Schrödinger equation. If $(20\nu_{\max})^{-1} < \delta t$ then integration of the electronic Schrödinger equation from t to $t + \delta t$ was performed over a series of smaller time steps of length $(20\nu_{\max})^{-1}$. Note that regardless of the size of $(20\nu_{\max})^{-1}$, hops were only considered at the end of the full time step from t to $t + \delta t$.

Let us first discuss the case of exact dynamics. The linear absorption spectra of the three-state models obtained using full quantum dynamics are shown as the solid black curves in Figure 5. Note that in order to highlight the relevant spectral features, we have not used consistent axis scales throughout all six panels. In the low diabatic coupling limit, $V_{23} = 0.0001$ hartree, the spectral features are all sharp indicating that the spectrum is dominated by transitions between bound states and suggesting that the dissociative diabat has little impact on the excited state dynamics. Indeed, the linewidths in this spectrum are primarily due to the truncation of Eq. (25) at finite $t_{\max}$. As V_{23} is increased, the central spectral feature near $\hbar\omega = 0.1$ hartree systematically broadens, indicating the increasing importance of the dissociative state and its inherent lifetime in the excited state dynamics. The resulting lifetime broadening becomes especially severe once $V_{23} = 0.005$ hartree, where the central feature spans over 0.02 hartree. Interestingly, the feature near $\hbar\omega = 0.115$ hartree, which is attributed to transitions to the first vibrationally excited state on the bright diabat, remains relatively sharp. Further increasing V_{23} to 0.01 hartree causes the spectrum to become even more substantially broadened, with the feature near $\hbar\omega = 0.115$ hartree nearly subsumed in the overall spectral envelope.

We now turn to the case of semiclassical dynamics. The semiclassical spectra obtained from FSSH trajectories using Eqs. (23) and (24) are also shown in Figure 5 as the dotted red curves. In the low diabatic coupling limit, the semiclassical spectrum agrees nearly quantitatively with the exact spectrum. This reflects the fact that in the limit $V_{23} \to 0$, the three-state model reduces to that of two shifted harmonic potentials with $\omega_g = \omega_e$ for which our semiclassical approach is exact. As V_{23} is increased, the agreement between the spectra calculated semiclassically and using full quantum dynamics loses some accuracy. However, our semiclassical approach is able to capture much of the overall lineshapes and spectral breadths as well as reproduce the trends in how the spectra evolve with increasing V_{23}. We believe that the deviations present can be attributed to the neglect of nuclear quantum effects, including decoherence and recoherences. Note that the relative importance of nuclear quantum effects and the long

time behavior of $C_{\mu\mu}(t)$ to the linear absorption spectra is increased in these model systems by the absence of environmental interactions and multiple vibrational degrees of freedom. As such, this study represents an especially challenging test of our semiclassical approach.

Figure 5 also presents spectra calculated using the ground-state Kubo approach in both the diabatic (dashed-dotted-dashed green lines) and adiabatic (dashed blue lines) representations.[9,10] Note that the presence of two coupled excited electronic states precludes us from also considering the application of Eq. (6) to this model system. In the diabatic representation, the dissociative state does not enter into the Kubo calculations and therefore the resulting spectra are independent of V_{23} and calculated using Eq. (5). As shown in panel (a) of Figure 5, even when V_{23} is very small, the diabatic ground-state Kubo spectrum is shifted significantly from the results of full quantum dynamics and exhibits a qualitatively incorrect overall spectral pattern. In the adiabatic representation, a Kubo approach must take into account the position dependence of the adiabatic transition dipole moment and the fact that two adiabatic excited states are coupled to the ground state. To do so, we define

$$\begin{aligned} C_{\mu\mu}^{(\text{Kubo adiab})}(t) &= \frac{\left|\mu_{21}^{(\text{diab})}\right|^2}{N_{\text{traj}}} \sum_{\ell=1}^{N_{\text{traj}}} U_{22}(x^{(1)[\ell]}(t)) U_{22}(x^{(1)[\ell]}(0)) \exp\left[-\frac{i}{\hbar}\int_0^t dt'(\mathbb{E}_2(x^{(1)[\ell]}(t')) - \mathbb{E}_1(x^{(1)[\ell]}(t')))\right] \\ &+ \frac{\left|\mu_{21}^{(\text{diab})}\right|^2}{N_{\text{traj}}} \sum_{\ell=1}^{N_{\text{traj}}} U_{23}(x^{(1)[\ell]}(t)) U_{23}(x^{(1)[\ell]}(0)) \exp\left[-\frac{i}{\hbar}\int_0^t dt'(\mathbb{E}_3(x^{(1)[\ell]}(t')) - \mathbb{E}_1(x^{(1)[\ell]}(t')))\right], \end{aligned} \tag{30}$$

where $\mathbb{E}_k(x)$ is the kth adiabatic potential and we have used the fact that $\mathbf{U}(x)$ is real for these systems. As shown in Figure 5, when $V_{23} = 0.0001$ hartree, the adibatic ground-state Kubo spectrum is qualitatively similar to the Kubo spectrum calculated in the diabatic representation (which is incorrect). As V_{23} is increased to 0.001 hartree, the agreement of the adiabatic Kubo spectrum with the results of full quantum dynamics does not significantly improve. Further increasing V_{23} does shift the central peak position in the adiabatic Kubo spectrum into the correct region but the adiabatic Kubo lineshapes remain qualitatively different from those in the exact spectra. In particular, the central peak is much too sharp, having maximum amplitudes of 34.71 and 18.87 for $V_{23} = 0.005$ hartree and $V_{23} = 0.01$ hartree, respectively. Finally, we emphasize that our semiclassical approach (Eqs. (23) and (24)) produces linear absorption spectra that are in much better agreement with the results of full quantum dynamics than what is obtained from the ground-state Kubo formalism.

V. CONCLUSION

In this paper, we have described a surface hopping approach for calculating dipole-dipole correlation functions based on averaging together information obtained from independent swarms of trajectories evolved on the ground and excited PESs. This approach was inspired by our recent progress connecting the FSSH algorithm to a rigorous nuclear-electronic density matrix.[48,49] For the specific model of two shifted harmonic potentials with equal harmonic frequencies and in the absence of electronic relaxation, we demonstrated that our approach yields an exact expression for the dipole-dipole correlation function.[13,14] When the two shifted harmonic potentials have different harmonic frequencies or when anharmonicity is introduced into the potentials, our method significantly outperforms the ground-state Kubo approach (Eq. (5)) and is comparable to the semiclassical formalism of evolving the trajectories on the mean surface (Eq. (6)).[9–11] For a model problem involving electronic relaxation, specifically a three-state model in which the bright excited state is vibronically coupled with a dark excited state, we demonstrated that our semiclassical approach is able to capture the effects of non-adiabatic, excited state dynamics on linear absorption spectra and deliver relatively accurate lifetime broadening. Furthermore, we demonstrated that Eqs. (23) and (24) significantly outperform both the adiabatic and diabatic ground-state Kubo approaches.

It is important to realize that all of the model systems considered in this study were gas (as opposed to condensed) phase. Without the presence of an environment with which to interact, all bound state dynamics are fully time-reversal and correlation functions do not decay. As a result, a short time approximation to the evolution of $C_{\mu\mu}(t)$ is not good enough. Therefore, the fact that the long time dynamics of Eq. (24) do not formally agree with a rigorous semiclassical analysis of Eq. (3) (as shown in Appendix B) will be a source of errors in our approach. Furthermore, because we are measuring the overlap between wave packets on different surfaces that separate and then come back together, these spectroscopic calculations display some of the decoherence/recoherence effects that we cannot fully capture in any FSSH-like description using independent trajectories.[43,48] Note, though, that for the systems considered in this study, the ground and excited state wave packets never formally interact through a derivative coupling after $t = 0$ and therefore the FSSH algorithm is formally applicable (see Appendix C). The ability of our FSSH-based method to successfully replicate so many of the features in the linear absorption spectra of these gas phase systems despite the above challenges give us confidence that it will provide a

reliable tool for modeling electronic spectra in the condensed phase.

A more exhaustive benchmarking of our method over a larger range of parameters of the three-state model introduced above is currently underway and will be reported in a follow-up paper. In particular, we have noticed that our approach becomes less accurate when V_{23} is large and the diabatic curve crossing occurs in the center of the Franck-Condon region and we are currently working on determining the cause of this. Additional benchmarking calculations are being performed on model systems that include environmental interactions as well as multiple bright electronic states in the diabatic representation. We are also exploring the effect of introducing decoherence into the dynamics through our group's augmented fewest switches surface hopping algorithm (AFFSH).[43,48] In doing so, it will be interesting to consider whether the effects of recoherences can, at least partially, be captured by modifying how the electronic wave functions are collapsed within AFFSH. We aim to apply these ideas to the calculation of spectral lineshapes in realistic, condensed phase systems in the near future.

ACKNOWLEDGMENTS

This material is based upon work supported by the (U.S.) Air Force Office of Scientific Research (USAFOSR) PECASE award under AFOSR Grant No. FA9950-13-1-0157. J.E.S. acknowledges an Alfred P. Sloan Research Fellowship and a David and Lucille Packard Fellowship.

APPENDIX A: EQUATION (9) IS EXACT FOR TWO UNCOUPLED, SHIFTED HARMONIC POTENTIALS WITH IDENTICAL HARMONIC FREQUENCIES AT NON-ZERO TEMPERATURES

We demonstrate here that Eq. (9) is exact for the model problem of two shifted harmonic potentials (Eq. (10)) with identical frequencies at non-zero temperatures. This only differs from the derivation presented in the main text in that the initial conditions of the classical trajectories must now be sampled from the finite temperature harmonic oscillator Wigner distribution.[1] The ensemble averaging is therefore accomplished according to

$$\begin{aligned}
&\left\langle \exp\left[-\frac{i}{\hbar}(Dp_0\cos(\omega t) - Dp_0 - m\omega Dx_0\sin(\omega t))\right]\right\rangle_{g,T\neq 0} \\
&= \int_{-\infty}^{\infty} dp_0 \int_{-\infty}^{\infty} dx_0 \exp\left[-\frac{i}{\hbar}\Big(Dp_0\left(\cos(\omega t)-1\right) - m\omega Dx_0\sin(\omega t)\Big)\right] \\
&\quad \times \frac{\tanh(\hbar\omega\beta/2)}{\hbar\pi}\exp\left[-\frac{\tanh(\hbar\omega\beta/2)p_0^2}{m\omega\hbar} - \frac{\tanh(\hbar\omega\beta/2)m\omega x_0^2}{\hbar}\right] \\
&= \exp\left[\frac{m\omega D^2}{2\hbar\tanh(\hbar\omega\beta/2)}(\cos(\omega t)-1)\right].
\end{aligned} \tag{A1}$$

The $T > 0$ electronic density matrix elements are therefore

$$\begin{aligned}
\frac{\left\langle\sigma_{eg}^{(g)}(t)\right\rangle_g}{\sigma_{eg}(0)} &= \exp\left[-\frac{i\epsilon_0 t}{\hbar} - \frac{im\omega^2 D^2 t}{2\hbar}\right]\exp\left[\frac{m\omega D^2}{2\hbar\tanh\left(\hbar\omega\beta/2\right)}\left(\cos(\omega t)-1\right)\right], \\
\frac{\left\langle\sigma_{eg}^{(e)}(t)\right\rangle_g}{\sigma_{eg}(0)} &= \exp\left[-\frac{i\epsilon_0 t}{\hbar} + \frac{im\omega^2 D^2 t}{2\hbar} - \frac{im\omega D^2\sin(\omega t)}{\hbar}\right]\exp\left[\frac{m\omega D^2}{2\hbar\tanh\left(\hbar\omega\beta/2\right)}\left(\cos(\omega t)-1\right)\right],
\end{aligned} \tag{A2}$$

and the dipole-dipole correlation function calculated using Eq. (9) is

$$C_{\mu\mu}(t) = |\mu_{eg}|^2\exp\left[-\frac{i\epsilon_0 t}{\hbar} - \frac{im\omega D^2}{2\hbar}\sin(\omega t)\right]\exp\left[\frac{m\omega D^2}{2\hbar\tanh\left(\hbar\omega\beta/2\right)}(\cos(\omega t)-1)\right]. \tag{A3}$$

The analytic expression for $C_{\mu\mu}(t)$ with $T > 0$ for this system is commonly written as[13,14]

$$\begin{aligned}
C_{\mu\mu}(t) &= |\mu_{eg}|^2\exp\left[-\frac{i\epsilon_0 t}{\hbar}\right]\exp\left[\frac{m\omega D^2}{2\hbar}\left(\left(\frac{1}{e^{\beta\hbar\omega}-1}+1\right)\left(e^{-i\omega t}-1\right) + \frac{1}{e^{\beta\hbar\omega}-1}\left(e^{i\omega t}-1\right)\right)\right] \\
&= |\mu_{eg}|^2\exp\left[-\frac{i\epsilon_0 t}{\hbar}\right]\exp\left[-\frac{im\omega D^2\sin(\omega t)}{2\hbar}\right]\exp\left[\frac{m\omega D^2}{2\hbar}\left(\cos(\omega t)-1\right)\left(1+\frac{2}{e^{\beta\hbar\omega}-1}\right)\right],
\end{aligned} \tag{A4}$$

which is identical to Eq. (A3).

APPENDIX B: SHORT TIME JUSTIFICATION FOR EQ. (9)

Consider a system with two-electronic states, g and e, in the presence of electronic relaxation. As described in Sec. III, there are two definitions for the off-diagonal elements of the mixed quantum-classical nuclear-electronic density matrix consistent with an ensemble of FSSH trajectories, $A^{(g)}_{ge}(\vec{x},\vec{p},t)$ and $A^{(e)}_{ge}(\vec{x},\vec{p},t)$, given in Eq. (20); these definitions differ by whether the trajectories are propagated on the ground or excited PESs. The time evolution of the geometric mean of $A^{(g)}_{ge}(\vec{x},\vec{p},t)$ and $A^{(e)}_{ge}(\vec{x},\vec{p},t)$, which underlies the expression for the dipole-dipole correlation function presented in Eqs. (23) and (24), is given by

$$\frac{d}{dt}\sqrt{A^{(e)}_{ge}(\vec{x},\vec{p},t)A^{(g)}_{ge}(\vec{x},\vec{p},t)} = \frac{1}{2\sqrt{A^{(e)}_{ge}(\vec{x},\vec{p},t)A^{(g)}_{ge}(\vec{x},\vec{p},t)}}\left[A^{(e)}_{ge}(\vec{x},\vec{p},t)\frac{\partial A^{(g)}_{ge}(\vec{x},\vec{p},t)}{\partial t} + A^{(g)}_{ge}(\vec{x},\vec{p},t)\frac{\partial A^{(e)}_{ge}(\vec{x},\vec{p},t)}{\partial t}\right]. \quad \text{(B1)}$$

The equations of motion for $A^{(g)}_{ge}(\vec{x},\vec{p},t)$ and $A^{(e)}_{ge}(\vec{x},\vec{p},t)$ were derived in a recent study performed in our group and shown to be[48]

$$\begin{aligned}
\frac{\partial A^{(g)}_{ge}(\vec{x},\vec{p},t)}{\partial t} &= \frac{-i}{\hbar}(V_{gg}-V_{ee})A^{(g)}_{ge} - \frac{p^\alpha d^\alpha_{ge}}{m^\alpha}(A_{ee}-A_{gg}) - \frac{p^\alpha}{m^\alpha}\frac{\partial A^{(g)}_{ge}}{\partial x^\alpha} - F^\alpha_{gg}\frac{\partial A^{(g)}_{ge}}{\partial p^\alpha} - \left(\frac{\partial A^{(e)}_{eg}}{\partial p^\alpha}F^\alpha_{ge} + F^\alpha_{eg}\frac{\partial A^{(e)}_{ge}}{\partial p^\alpha}\right)\frac{\sigma^{(g)}_{ge}}{\sigma^{(g)}_{gg}}\zeta^+, \\
\frac{\partial A^{(e)}_{ge}(\vec{x},\vec{p},t)}{\partial t} &= \frac{-i}{\hbar}(V_{gg}-V_{ee})A^{(e)}_{ge} - \frac{p^\alpha d^\alpha_{ge}}{m^\alpha}(A_{ee}-A_{gg}) - \frac{p^\alpha}{m^\alpha}\frac{\partial A^{(e)}_{ge}}{\partial x^\alpha} - F^\alpha_{ee}\frac{\partial A^{(e)}_{ge}}{\partial p^\alpha} - \left(\frac{\partial A^{(g)}_{eg}}{\partial p^\alpha}F^\alpha_{ge} + F^\alpha_{eg}\frac{\partial A^{(g)}_{ge}}{\partial p^\alpha}\right)\frac{\sigma^{(e)}_{ge}}{\sigma^{(e)}_{ee}}\zeta^-,
\end{aligned} \quad \text{(B2)}$$

where, for brevity, the dependence of the various terms on $\vec{x}$ and $\vec{p}$ has not been explicitly shown. A superscript α is used to denote a specific nuclear coordinate and summation over all nuclear degrees of freedom is implied when α appears two or more times within a term. The αth component of the force on the ground PES is given by $F^\alpha_{gg}(\vec{x})$, the derivative couplings are $d^\alpha_{ge}(\vec{x}) = \langle\Phi_g(\vec{x})|\frac{\partial}{\partial x^\alpha}|\Phi_e(\vec{x})\rangle$, and the off-diagonal forces satisfy $F^\alpha_{ge}(\vec{x}) = d^\alpha_{ge}(\vec{x})(V_{gg}(\vec{x})-V_{ee}(\vec{x}))$. Finally, ζ^+ and ζ^- are Heaviside functions, the arguments of which are given in Subotnik *et al.*[48]

At the start of the simulation, $A^{(g)}_{ge}(\vec{x},\vec{p},0) = A^{(e)}_{ge}(\vec{x},\vec{p},0)$. However, because the two equations of motion in Eq. (B2) are different, $A^{(g)}_{ge}(\vec{x},\vec{p},t)$ and $A^{(e)}_{ge}(\vec{x},\vec{p},t)$ will diverge from each other as the simulation proceeds. However, if we focus on the short time behavior of $\mathbf{A}(\vec{x},\vec{p},t)$, then $A^{(g)}_{ge}(\vec{x},\vec{p},t) \simeq A^{(e)}_{ge}(\vec{x},\vec{p},t) \equiv A_{ge}(\vec{x},\vec{p},t)$ and

$$\begin{aligned}
&\frac{d}{dt}\sqrt{A^{(e)}_{ge}A^{(g)}_{ge}} \\
&\simeq \frac{-i}{2\hbar}(V_{gg}-V_{ee})A_{ge} - \frac{p^\alpha d^\alpha_{ge}}{2m^\alpha}(A_{ee}-A_{gg}) - \frac{p^\alpha}{2m^\alpha}\frac{\partial A_{ge}}{\partial x^\alpha} - \frac{F^\alpha_{gg}}{2}\frac{\partial A_{ge}}{\partial p^\alpha} \\
&\quad - \left(\frac{\partial A_{eg}}{\partial p^\alpha}F^\alpha_{ge} + F^\alpha_{eg}\frac{\partial A_{ge}}{\partial p^\alpha}\right)\frac{\sigma_{ge}}{2\sigma_{gg}}\zeta^+ + \frac{-i}{2\hbar}(V_{gg}-V_{ee})A_{ge} - \frac{p^\alpha d^\alpha_{ge}}{2m^\alpha}(A_{ee}-A_{gg}) \\
&\quad - \frac{p^\alpha}{2m^\alpha}\frac{\partial A_{ge}}{\partial x^\alpha} - \frac{F^\alpha_{ee}}{2}\frac{\partial A_{ge}}{\partial p^\alpha} - \left(\frac{\partial A_{eg}}{\partial p^\alpha}F^\alpha_{ge} + F^\alpha_{eg}\frac{\partial A_{ge}}{\partial p^\alpha}\right)\frac{\sigma_{ge}}{2\sigma_{ee}}\zeta^- \\
&= \frac{-i}{\hbar}(V_{gg}-V_{ee})A_{ge} - \frac{p^\alpha d^\alpha_{ge}}{m^\alpha}(A_{ee}-A_{gg}) - \frac{p^\alpha}{m^\alpha}\frac{\partial A_{ge}}{\partial x^\alpha} - \frac{F^\alpha_{ee}+F^\alpha_{gg}}{2}\frac{\partial A_{ge}}{\partial p^\alpha} \\
&\quad - \frac{1}{2}\left(\frac{\partial A_{eg}}{\partial p^\alpha}F^\alpha_{ge} + F^\alpha_{eg}\frac{\partial A_{ge}}{\partial p^\alpha}\right)\left(\frac{\sigma_{ge}}{\sigma_{gg}}\zeta^+ + \frac{\sigma_{ge}}{\sigma_{ee}}\zeta^-\right).
\end{aligned} \quad \text{(B3)}$$

From Eq. (B3), we see that, at least for short times, the evolution of $\sqrt{A^{(e)}_{ge}(\vec{x},\vec{p},t)A^{(g)}_{ge}(\vec{x},\vec{p},t)}$ is consistent with propagating trajectories on the mean potential, as evident by the presence of the $\frac{1}{2}(F^\alpha_{gg}+F^\alpha_{ee})\partial A_{ge}/\partial p^\alpha$ term. Propagation on the mean potential matches the dynamics from a rigorous, semiclassical analysis of Eq. (3).[11,15,17,23]

APPENDIX C: A COMMENT ON RECOHERENCES

It is important to realize that the term "recoherence" can actually refer to two slightly different phenomenon. On the one hand, we might have the situation where (1) two wave packets begin on the same PES, (2) one of these wave packets branches off to another adiabatic PES due to derivative

coupling, (3) both wave packets evolve on their separate surfaces until (4) one of the wave packets encounters another derivative coupling region so that (5) both wave packets end up on the same PES. If the two wave packets are in the same region of configuration space when this occurs, then they will interfere and this interference is identified as a recoherence. Such a recoherence is absolutely not describable by FSSH because it violates the underlying unique trajectory assumption.[48]

On the other hand, "recoherence" can also refer to the time dependent overlap of nuclear wave packets moving on different PESs. This process is one that FSSH could fully describe if interacting trajectories were used. With non-interacting trajectories, such recoherences can only be approximated by FSSH. However, the results presented in this study seem to indicate that swarms of non-interacting FSSH trajectories propagated on the ground and excited PESs can provide a surprisingly robust approximation for this second definition of wave packet recoherence.

[1] D. J. Tannor, *Introduction to Quantum Mechanics: A Time Dependent Perspective* (University Science Press, Sausalito, 2007).
[2] E. J. Heller, Acc. Chem. Res. **14**, 368 (1981).
[3] M. Ben-Nun and T. J. Martínez, J. Phys. Chem. A **103**, 10517 (1999).
[4] W. H. Miller, J. Phys. Chem. A **105**, 2942 (2001).
[5] H. Wang and M. Thoss, Chem. Phys. **304**, 121 (2004).
[6] Q. Shi and E. Geva, J. Chem. Phys. **122**, 064506 (2005).
[7] P. L. McRobbie and E. Geva, J. Phys. Chem. A **113**, 10425 (2009).
[8] S. A. Egorov, E. Rabani, and B. J. Berne, J. Chem. Phys. **108**, 1407 (1998).
[9] R. Kubo, Adv. Chem. Phys. **15**, 101 (1969).
[10] J. G. Saven and J. L. Skinner, J. Chem. Phys. **99**, 4391 (1993).
[11] N. E. Shemetulskis and R. F. Loring, J. Chem. Phys. **97**, 1217 (1992).
[12] C. Spencer and R. F. Loring, J. Chem. Phys. **105**, 6596 (1996).
[13] A. Nitzan, *Chemical Dynamics in Condensed Phases* (Oxford University Press, 2006).
[14] S. Mukamel, *Principles of Nonlinear Optical Spectroscopy* (Oxford University Press, 1995).
[15] S. Mukamel, J. Chem. Phys. **77**, 173 (1982).
[16] M. Wehrle, M. Šulc, and J. Vaníček, Chimia **65**, 334 (2011).
[17] M. Šulc, H. Hernández, T. J. Martínez, and J. Vaníček, J. Chem. Phys. **139**, 034112 (2013).
[18] F. Webster, J. Schnitker, M. Friedrichs, R. A. Friesner, and P. J. Rossky, Phys. Rev. Lett. **66**, 3172 (1991).
[19] L. Turi, H. Gyoergy, P. J. Rossky, and D. Borgis, J. Chem. Phys. **131**, 024119 (2009).
[20] O. Kühn and N. Makri, J. Phys. Chem. A **103**, 9487 (1999).
[21] N. Rekik, C.-Y. Hsieh, H. Freedman, and G. Hanna, J. Chem. Phys. **138**, 144106 (2013).
[22] G. Hanna and E. Geva, J. Phys. Chem. B **115**, 5191 (2011).
[23] R. Kapral and G. Ciccotti, J. Chem. Phys. **110**, 8919 (1999).
[24] C. C. Martens, Int. J. Quant. Chem. **113**, 316 (2013).
[25] J. C. Tully, J. Chem. Phys. **93**, 1061 (1990).
[26] G. Stock and M. Thoss, Phys. Rev. Lett. **78**, 578 (1997).
[27] M. Ben-Nun, J. Quenneville, and T. J. Martínez, J. Phys. Chem. A **104**, 5161 (2000).
[28] W. H. Miller, J. Phys. Chem. A **113**, 1405 (2009).
[29] G. A. Jones, B. K. Carpenter, and M. N. Paddon-Row, J. Am. Chem. Soc. **120**, 5499 (1998).
[30] A. Hazra, A. V. Soudackov, and S. Hammes-Schiffer, J. Phys. Chem. B **114**, 12319 (2010).
[31] D. Nachtigallová, A. J. A. Aquino, J. J. Szymczak, M. Barbatti, P. Hobza, and H. Lischka, J. Phys. Chem. A **115**, 5247 (2011).
[32] G. Granucci and M. Persico, J. Chem. Phys. **126**, 134114 (2007).
[33] S. Fernandez-Alberti, V. D. Kleiman, S. Tretiak, and A. E. Roitberg, J. Phys. Chem. A **113**, 7535 (2009).
[34] W. Domcke and D. R. Yarkony, Annu. Rev. Phys. Chem. **63**, 325 (2012).
[35] *Conical Intersections: Electronic Structure, Dynamics, and Spectroscopy*, edited by W. Domcke, D. R. Yarkony, and H. Köppel (World Scientific Publishing Co. Pte. Ltd., 2004).
[36] R. Mitrić, J. Petersen, and V. Bonačić-Koutecký, Phys. Rev. A **79**, 053416 (2009).
[37] M. Richter, P. Marquetand, J. González-Vázquez, I. Sola, and L. González, J. Chem. Theory Comput. **7**, 1253 (2011).
[38] J. J. Bajo, J. González-Vázquez, I. R. Sola, J. Santamaria, M. Richter, P. Marquetand, and L. González, J. Phys. Chem. A **116**, 2800 (2012).
[39] U. Müller and M. Thoss, J. Chem. Phys. **107**, 6230 (1997).
[40] A. Kelly and T. E. Markland, J. Chem. Phys. **139**, 014104 (2013).
[41] L. Wang and D. Beljonne, J. Chem. Phys. **139**, 064316 (2013).
[42] W. Xie, S. Bai, and Q. Shi, J. Phys. Chem. A **117**, 6196 (2013).
[43] B. R. Landry and J. E. Subotnik, J. Chem. Phys. **137**, 22A513 (2012).
[44] R. Tempelaar, C. P. van der Vegte, J. Knoester, and T. L. C. Jansen, J. Chem. Phys. **138**, 164106 (2013).
[45] C. C. Martens and J. Y. Fang, J. Chem. Phys. **106**, 4918 (1997).
[46] A. Donoso and C. C. Martens, J. Phys. Chem. A **102**, 4291 (1998).
[47] S. Nielsen, R. Kapral, and G. Ciccotti, J. Chem. Phys. **112**, 6543 (2000).
[48] J. E. Subotnik, W. Ouyang, and B. R. Landry, J. Chem. Phys. **139**, 214107 (2013).
[49] B. R. Landry, M. J. Falk, and J. E. Subotnik, J. Chem. Phys. **139**, 211101 (2013).
[50] E. Wigner, Phys. Rev. **40**, 749 (1932).
[51] W. B. Case, Am. J. Phys. **76**, 937 (2008).
[52] J. C. Tully, Faraday Discuss. **110**, 407 (1998).
[53] G. A. Worth, H.-D. Meyer, and L. S. Cederbaum, in *Conical Intersections: Electronic Structure, Dynamics, and Spectroscopy*, edited by W. Domcke, D. R. Yarkony, and H. Köppel (World Scientific Publishing Co. Pte. Ltd., 2004), Chap. 14, pp. 619–698.
[54] W. Press, B. Flannery, S. Teukolsky, and W. Vetterling, *Numerical Recipes in FORTRAN 77: The Art of Scientific Computing*, Fortran Numerical Recipes Vol. 1 (Cambridge University Press, 1992).
[55] See supplementary material at http://dx.doi.org/10.1063/1.4884945 for a more exhaustive data set showing the performance of the various semiclassical approaches for the model system of two displaced harmonic potentials with $\omega_g \neq \omega_e$ at both zero-temperature and a range of finite temperatures.
[56] P. M. Morse, Phys. Rev. **34**, 57 (1929).
[57] D. T. Colbert and W. H. Miller, J. Chem. Phys. **96**, 1982 (1992).
[58] Q. Shi and E. Geva, J. Chem. Phys. **129**, 124505 (2008).
[59] P. L. McRobbie, G. Hanna, Q. Shi, and E. Geva, Acc. Chem. Res. **42**, 1299 (2009).